Finite Element Analysis to Compare the Accuracy of the Direct and MDEV Inversion Algorithms in MR Elastography

Lyam Hollis, Eric Barnhill, Noel Conlisk, Lauren E.J. Thomas-Seale, Neil Roberts, Pankaj Pankaj
and Peter R. Hoskins

Abstract—**Magnetic resonance elastography (MRE) utilises an inversion algorithm to create maps of material properties (elastograms) from displacements caused by mechanically induced shear waves. This study aimed to assess the accuracy of measurements from multi-dual elasto-visco (MDEV) inversion in comparison to direct inversion (DI) in simplistic geometries. Finite element analysis (FEA) was used to simulate wave propagation in cuboid geometries with embedded cylindrical inserts. Accuracy of both algorithms was dependent upon insert length, diameter and shear modulus. Whilst MDEV reduced artefacts in the elastograms in comparison to DI it was unable to improve accuracy of the measurements.**

Index Terms—**magnetic resonance elastography, finite element analysis, multi-frequency dual visco-elastic inversion, direct inversion.**

I. INTRODUCTION

MAGNETIC resonance elastography (MRE) is a technique developed to measure mechanical properties of tissue *in vivo* non-invasively [1], [2]. Typically a motion-encoding gradient is used to characterise the propagation of shear waves induced by an external harmonically oscillating source. An inversion algorithm is then utilised to attain the material properties from these displacements typically presented in the form of a spatial map known as an elastogram.

Currently the clinical use of MRE is confined to the diagnosis of hepatic fibrosis where it is able characterise a significant increase in shear stiffness of diseased liver in comparison to the healthy liver and increasing stiffness throughout the various stages of the disease [3]. The technique has been shown as more diagnostically accurate than ultrasound elastography and biopsy, the current gold standard technique [4]. Research into the technique now also focuses on a varied range of tissues including the kidneys [5], muscle [6], heart [7] and aorta [8]–[10].

Inversion of the displacement data can be performed in a number of different ways. Direct inversion (DI) [11] utilises the Laplace operator obtaining good resolution at the expense of low-signal-to-noise ratio [12]. Derivation of DI is based upon several key assumptions; that the medium is homogeneous, linearly elastic and isotropic [13]. These assumptions

L. Hollis, N. Conlisk, LEJ. Thomas-Seale and PR. Hoskins are with the Centre for Cardiovascular Sciences, University of Edinburgh, 47 Little France Crescent, Edinburgh, EH16 4TJ

E. Barnhill and N. Roberts are with the Clinical Research Imaging Centre, University of Edinburgh, 47 Little France Crescent, Edinburgh, EH16 4TJ.

P. Pankaj is with the School of Engineering, University of Edinburgh, The King's Buildings, EH9 3JL.

Corresponding author is L. Hollis, Email: lyamhollis@outlook.com.

imply that in reality, measurements using DI are also dependent upon the geometry of the medium under investigation [14]. An extension of DI more recently introduced is the multi-frequency dual elasto-visco (MDEV) inversion [15]. Again this utilises the Laplacian but combines information acquired at multiple frequencies to reduce frequency dependent artefacts and achieve increased spatial resolution. This approach has been shown to improve image quality [16], however the ability of the technique to accurately resolve material properties in comparison to DI has not been assessed.

This paper aims to investigate whether MDEV is able to achieve greater accuracy of material property measurements than DI in a variety of simplistic geometries. To achieve this finite element analysis (FEA), a commonly used technique in the field [17]–[19], has been employed. Since the methods of assessing newly developed software varies across the literature, the 3-D datasets from the models used in this study have been made publicly available with the intention that future developers can utilise these and compare the performance of their software with the other available techniques.

II. METHODS

FEA has been performed using *Abaqus/Explicit (Dassault Systeme Simulia Corp., Providence, Rhode Island, USA)* (figure 1).
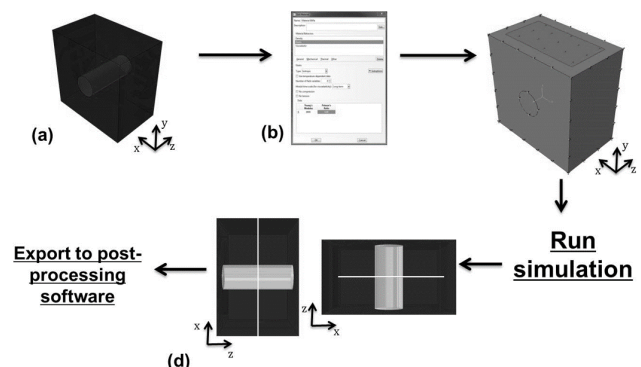

Fig. 1. Modelling workflow. (a) Creation of the geometry. (b) Assign the material properties. (c) Application of the load and assignment of boundary conditions. (d) Extraction of data from 2-dimensional plane.

A. Geometries

Models consisted of a cylindrical insert placed in an $100 \times 80 \times 80$ mm^3 cuboid background material. In order to

investigate the effects of out-of-plane geometries, the radius of the insert was maintained at 10 mm whilst the length was varied from 2-100 mm. To investigate the effects of in-plane geometry the length of the insert was fixed at 100 mm whilst the radii was varied from 5-30 mm (figure 2).
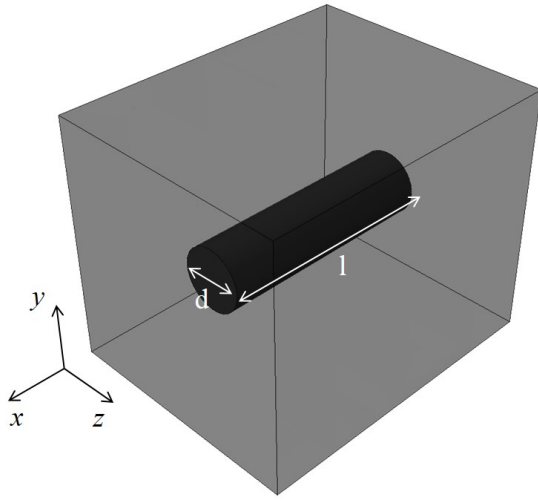

Fig. 2. Representation of the geometries used in this study. The length, l, and diameter, d, were varied to investigate the effect of out-of-plane and in-plane geometries respectively.

B. Material Properties

All materials used in this study were defined as viscoelastic using the Kelvin-Voigt model of viscoelasticity. The shear modulus of the background material was maintained at 3 kPa for all simulations whilst the insert was varied from 4-9 kPa. A shear viscosity of 1 Pa·s and density of 1047 kg·m^{-3} were defined throughout all materials which were assumed near incompressible with a Poissons ratio of 0.49.

C. Loading and Boundary Conditions

Vibrations were applied in the z-direction via a concentrated force acting upon a region of nodes on the upper surface (at $y=80$ mm) of the model. Frequencies of 50, 70 and 100 Hz were used. Displacements for all boundaries in the model excluding the surface upon which the load was applied were fixed in the y-direction. In all models the insert and background regions of the model were merged together as a single part.

D. Data Analysis

Data was extracted from 5 parallel slices 1 mm apart with pixel sizes in each slice of 1x1 mm^2. All three spatial directions were extracted independently of one another. The data was imported into *Matlab* where it was stored as three 4-D objects with the first three dimensions corresponding to x, y and z respectively and the fourth dimension corresponding to time. Each 4-D object corresponded to a different displacement direction.

Two approaches were used to invert the data. Firstly DI was performed in 3-dimensions using the direct solution to the Helmholtz equation:

$$G^* = -\rho\omega^2 \frac{\mathbf{u}}{\nabla^2 \mathbf{u}} \tag{1}$$

where ρ represents the density, ω is the angular frequency of excitation and $\mathbf{u}$ is the complex displacement field. G^* represents a complex number consisting of G', the storage modulus, and G'', the loss modulus, such that $G^* = G' + iG''$. When represented using polar co-ordinates in the complex plane (figure 3) this implies that:

$$G^* = |G^*|\left(\cos\phi + i\sin\phi\right) \tag{2}$$

such that:

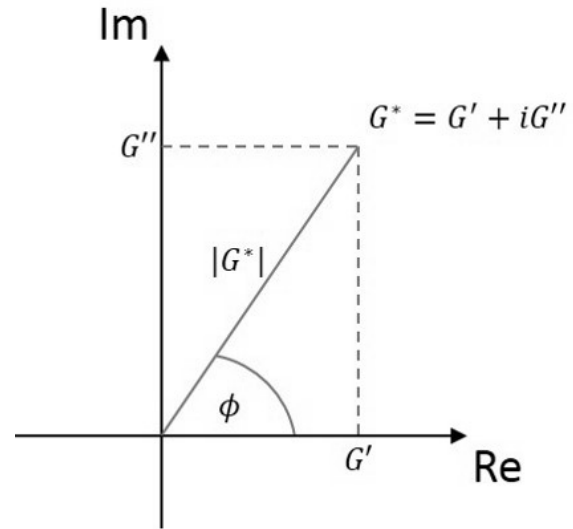$$\phi = \tan^{-1}\left(\frac{G''}{G'}\right) \tag{3}$$

Fig. 3. Illustration of the complex plane for G^*.

The second approach used was MDEV which utilises the Helmholtz equation but includes a summation over the frequencies to calculate $|G^*|$ [15]:

$$|G^*| = \rho\frac{\sum_{m=1}^{3}\sum_{n=1}^{N}\omega_n|u_m^*(\omega_n)|}{\sum_{m=1}^{3}\sum_{n=1}^{N}\nabla^2|u_m^*(\omega_n)|} \tag{4}$$

and ϕ:

$$\phi = \cos^{-1}\left(-\frac{\sum_{m=1}^{3}\sum_{n=1}^{N}\left[\Delta u_m'(\omega_n)u_m'(\omega_n)+\Delta u_m''(\omega_n)u_m''(\omega_n)\right]}{\sum_{m=1}^{3}\sum_{n=1}^{N}|\Delta u_m^*(\omega_n)||u_m^*(\omega_n)|}\right) \tag{5}$$

for N frequencies and the three spatial directions. In this way MDEV represents $|G^*|$ and ϕ as frequency independent variables [20].

Masks were applied to the background and insert regions and the mean value within this region measured (figure 4). In order to assess the accuracy of each algorithm the fractional error of the measured G' and G'' values to the assigned values was then calculated.
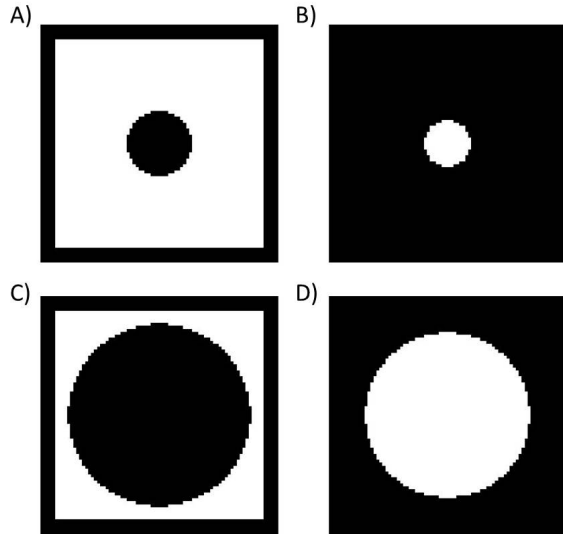
Fig. 4. Examples of the masks used to calculate mean $|G^*|$ values. A) and B) represent the masks used to calculate the background and insert respectively in models with an insert of radius 10 mm whilst C) and D) represent the masks to calculate the background and insert regions respectively in models with insert of radius 30 mm. The white represents the region of interest.

E. Wave Decomposition

In deriving the direct inversion algorithm, the influence of the compressional wave is often ignored. The validity of this assumption has, however, been the subject of dispute [21]. The influence of the compressional wave upon **u** can be approximated using Helmholtz decomposition, which states that the displacement field can be decomposed such that [22]:

$$\mathbf{u} = \nabla \times \Psi + \nabla \Phi \qquad (6)$$

Here Ψ and Φ represent vector and scalar potential fields corresponding to the shear and compressional waves respectively. Since the curl of the gradient function is equal to 0, as is the divergence of curl, this implies that:

$$\nabla \times \mathbf{u} = \nabla \times (\nabla \times \Psi)$$
$$\nabla \cdot \mathbf{u} = \nabla^2 \Phi \qquad (7)$$

For simplicity, let:

$$\psi = \nabla \times (\nabla \times \Psi)$$
$$\phi = \nabla^2 \Phi \qquad (8)$$

Application of these two operators does not, however, preserve the properties of the wavefield and resultantly the ampltiudes of the potentials are not comparable to one another [23]. This can be addressed by considering the velocities of the compressional and shear waves, with a balancing factor, α, to be defined as [24]:

$$\alpha = \frac{v_s}{v_c} \qquad (9)$$

where v_s and v_c are the velocities of the compressional and shear waves respectively. Assuming a linear elastic medium, the velocities are calculated as follows:

$$v_c = \sqrt{\frac{1}{\rho}\left(\frac{G}{1-2\upsilon} + \frac{4}{3}G\right)}$$

$$v_s = \sqrt{\frac{G}{\rho}} \qquad (10)$$

Although the medium is viscoelastic, and the velocity is also variable spatially in a non-uniform finite medium, these equations allow for an estimation of α throughout the model. As such, the fractional contribution, f, of the compressional wave to the total displacement can be approximated as:

$$f = \frac{|\phi|}{\alpha\,|\psi| + |\phi|} \qquad (11)$$

for each pixel in the complex wave image. This implies that if the wavefield is a pure shear field, the fractional contribution will be equal to 0, whereas if the field is purely compressional, the value will be equal to 1.

F. Convergence and Meshing

Convergence studies were performed on all geometries used here. Since the shear modulus calculated by DI is a function of the displacement, the convergence criteria is based upon these measurements, with convergence assumed to have been achieved if the measured values in both the background and insert change by less than 2% for a decrement in element size. For consistency all simulations were meshed using 1.25 mm^3 C3D10M elements, since this element size was within the convergence criteria for all geometries.

III. RESULTS

Fractional errors for the storage modulus of the insert were large for the smaller length and smaller diameter inserts. Increasing the length or radius resulted in an initial decrease in the fractional error, before these errors plateaued (figures 5 and 7). The length or diameter at which this plateau occurred and the fractional error itself were dependent upon the frequency and the shear modulus of the insert: the plateau occurred at larger radii and lengths for higher shear modulus and for DI at 50 Hz. Measurements of G' in the background were largely independent of the radius of the insert. The fractional error for the background measurements at 100 Hz was variable for insert length. Inspection of both the real and imaginary components of the complex wave image showed non-planar wave propagation below the insert which corresponded to large artefacts in the G' elastogram. MDEV improved the quality of the G' elastograms with reductions in the size and number of artefacts (figures 6 and 8). MDEV was not however capable of achieving more accurate measurements than all three frequencies, with the fractional error typically falling between the lowest and highest fractional error through DI.

Fractional errors were typically larger for the loss modulus than the storage modulus, with large overestimations typically occurring in both the background and insert regions at 50 Hz (figures 5 and 7). Increasing the insert length had little impact upon the fractional error in the background region, but caused an increase in the error insert region. This increase was more pronounced for higher prescribed insert shear moduli and at 50 Hz in comparison to the other frequencies inverted with DI. Increasing the radius of the insert increased the size of the fractional error in the background region; again this effect was pronounced at 50 Hz . Fractional errors varied largely with radius, though in all cases there were large overestimations for the 5 mm radius insert. G''
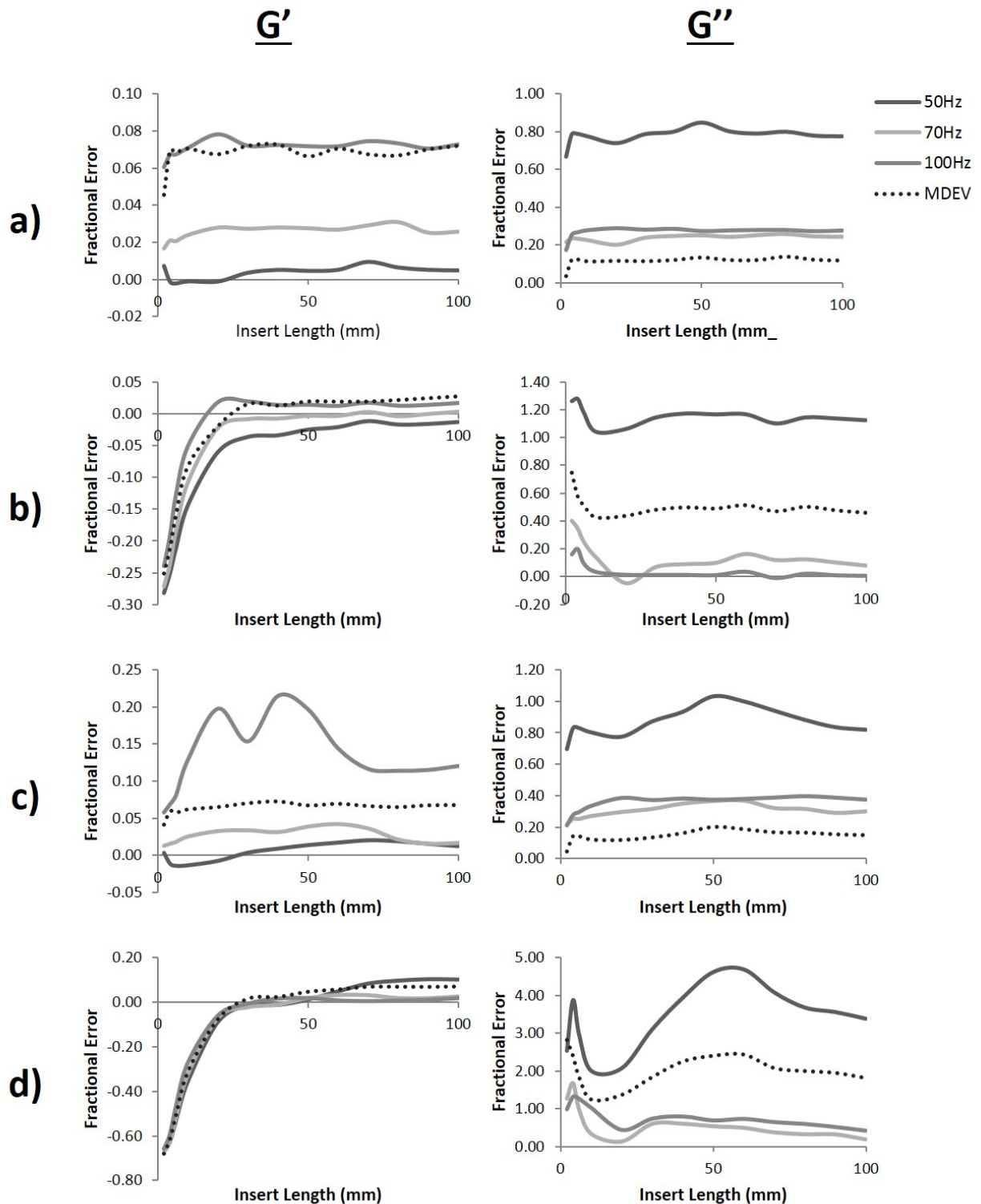
Fig. 5.   Examples of the fractional errors for variations in insert length. a) and b) represent the fractional errors in the background and insert measurements respectively for a 4 kPa 10 mm radius insert whilst c) and d) represent the fractional errors in the background and insert measurements respectively for a 9 kPa 10 mm radius insert. Both measurements of G' and G'' in the insert are dependent upon the length of the insert: whilst measurements of G' in the insert become more accurate with increasing length, the opposite is true of the measurements of G''. Accuracy of the measurements was not improved by using MDEV in comparison to DI.
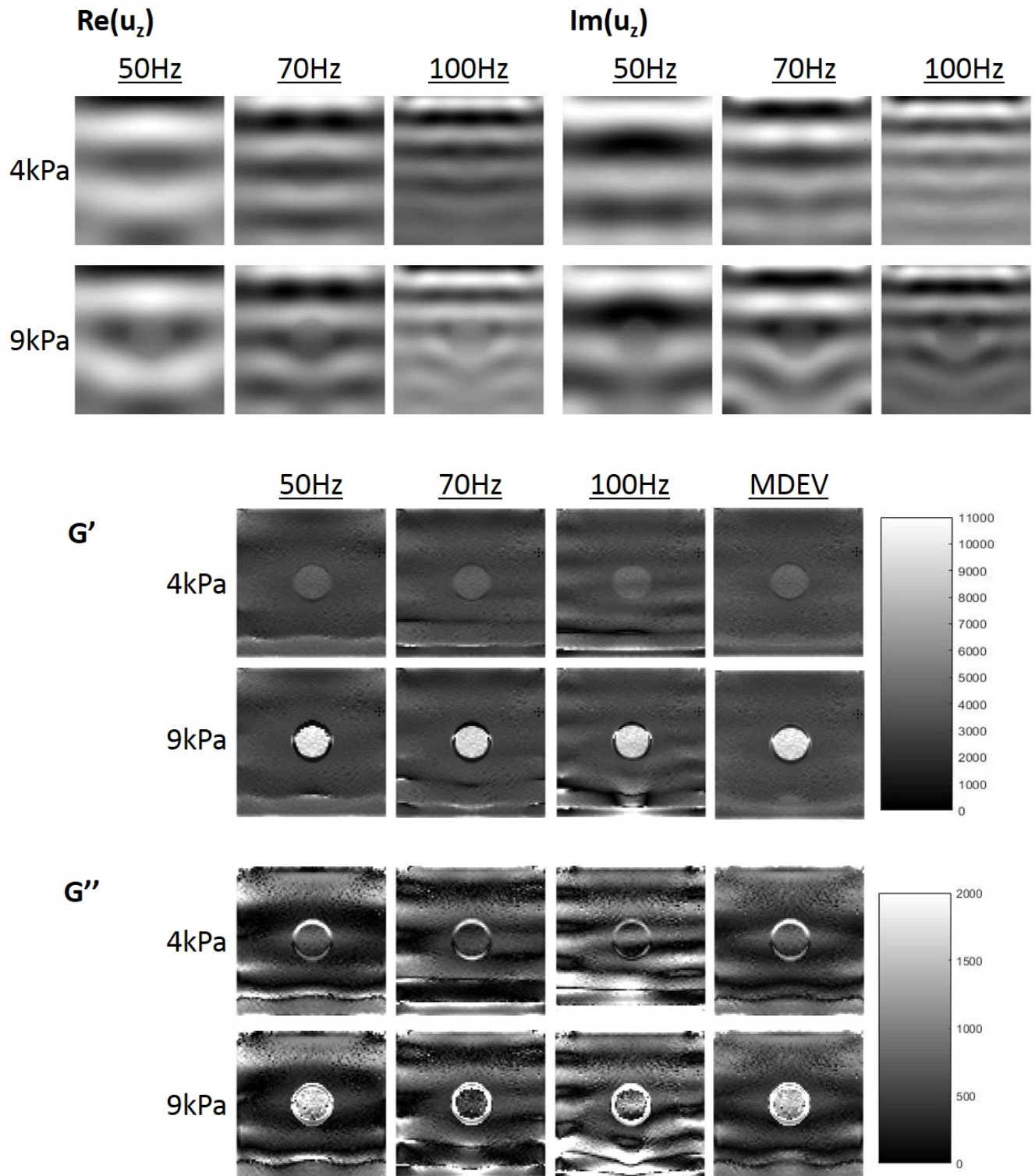
Fig. 6. Real and imaginary components of the complex displacements and the G' and G'' elastograms for the 4 and 9 kPa inserts for the 10 mm radius, 100 m length insert. The quality of both the G' and G'' elastograms are improved by MDEV in comparison to DI, which suffer from frequency dependent artefacts.
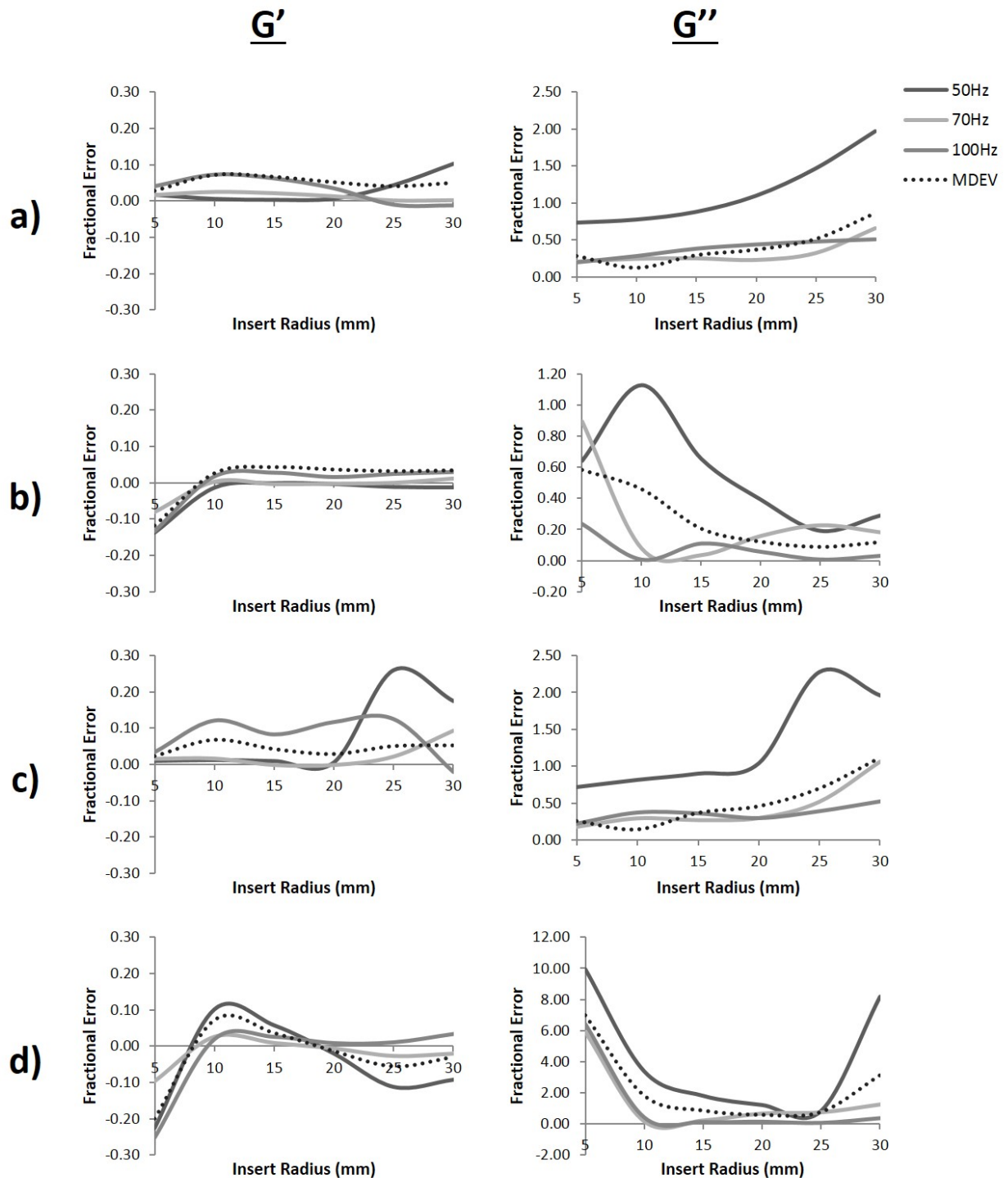
Fig. 7. Examples of the fractional errors for variations in insert radius. a) and b) represent the fractional errors in the background and insert measurements respectively for a 4 kPa 100 mm length insert whilst c) and d) represent the fractional errors in the background and insert measurements respectively for a 9 kPa 100 mm length insert. Typically the fractional error in both G' and G'' decreases with increasing radius, although there is an increase in the fractional error in G'' at 50 Hz. Large diameter inserts result in large fractional errors for the background G' and G'' measurements at 50 and 70 Hz. MDEV was unable to improve the accuracy of the measurements in comparison to DI.
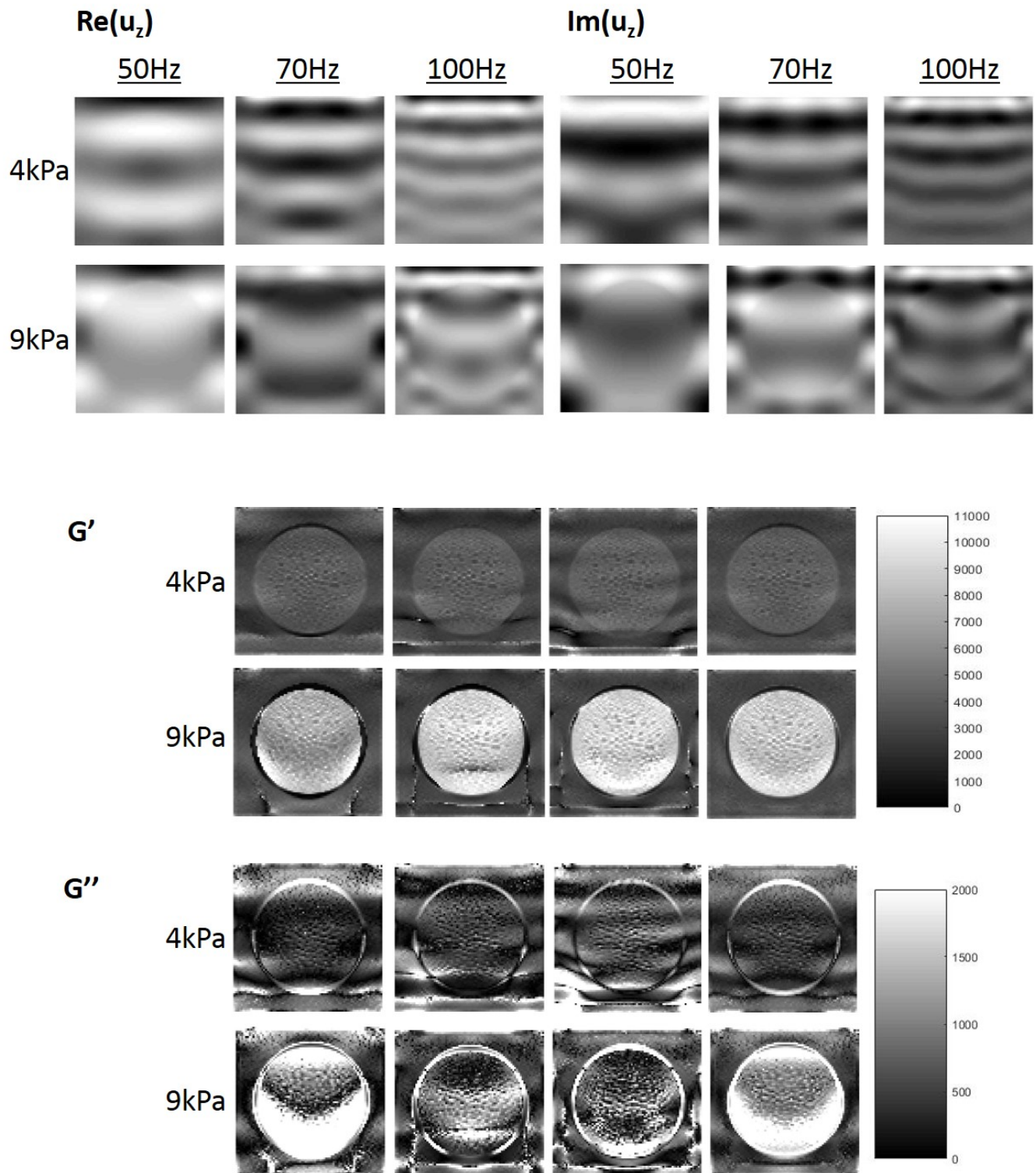
Fig. 8.   Real and imaginary components of the complex displacements and the G' and G'' elastograms for the 4 and 9 kPa inserts for the 30 mm radius, 100 m length insert. Whilst MDEV typically improved elastogram quality, artefacts at the boundary remained in the G'' elastogram. Frequency dependent artefacts were greatly reduced in the elastograms, but not always removed altogether. This is demonstrated well by the 9 kPa G'' elastogram, where the frequency dependent artefact from the 50 Hz DI is also clearly present following MDEV inversion.

elastograms constructed with DI were characterised by large artefacts (figures 6 and 8). The position of these artefacts was typically frequency dependent, however, an artefact appeared at the boundary between the background and the insert at all frequencies. Whilst MDEV reduced the frequency dependent artefacts, it was often unable to remove them all together. Artefacts at the background-insert boundary remained prominent following MDEV inversion. As with the storage modulus, fractional errors in the loss modulus from MDEV were typically between the lowest and highest fractional errors from DI for that region of interest.

The mean fractional contribution of the compressional wave to the displacement was typically in the range 0.1-0.25. This appeared to be largely independent of the length or diameter of the insert, with the exception of the 2 mm length insert model, where the mean fractional contribution was approximately 0.4 for all three frequencies. Inspection of the maps of the fractional contribution demonstrated that high values were typically associated with troughs in the x-component of the curl (figure 10).

Fig. 10. Maps showing the estimated fractional contribution of the compressional wave for the 100 mm length inserts of 10 mm radius, with a prescribed shear modulus of 9 kPa when vibrated at 50 and 100 Hz. The displacements are typically dominated by shear waves with high fractional contribution values occuring at the troughs for the x-component of the curl.
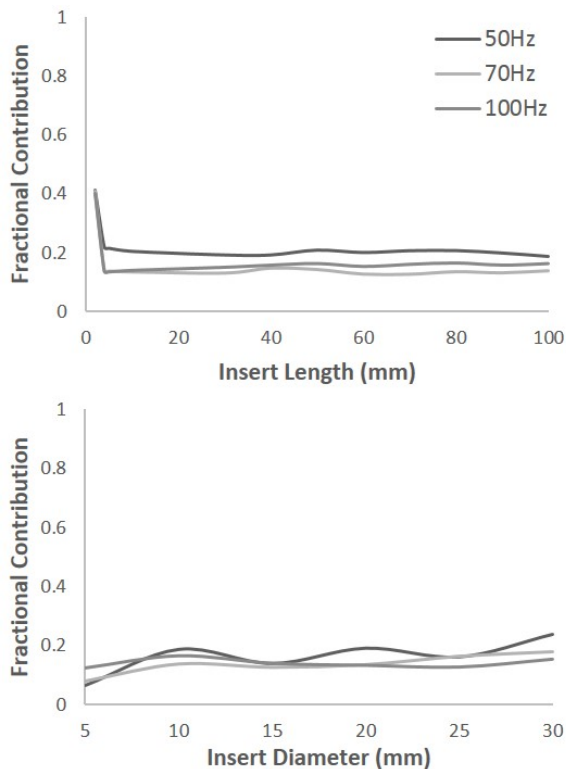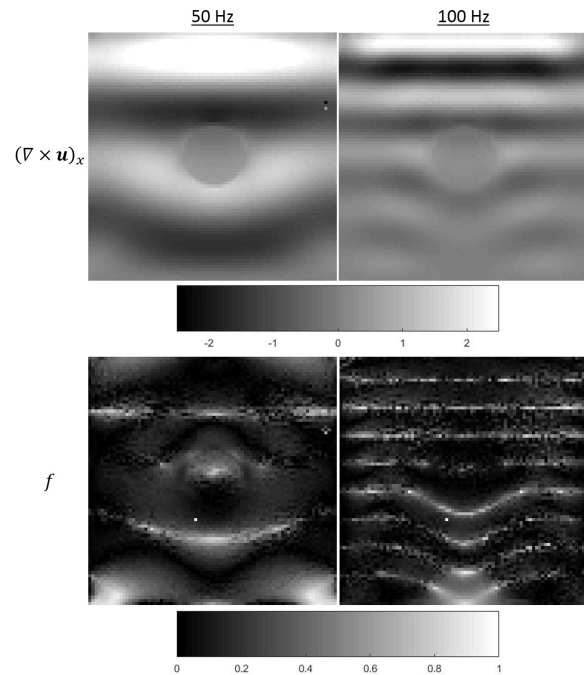

Fig. 9. Graphs demonstrating the mean fractional contribution of the compressional wave to the displacement throughout the model. In all cases the displacement is dominated by the contribution from the shear wave.

IV. DISCUSSION

All frequencies analysed individually by DI showed artefacts associated with scattering, reflections and viscoelastic damping [12]. Previous studies have demonstrated that since the positions of these artefacts are frequency independent, combining information from several frequencies using MDEV reduces their impact and results in improved quality of the elastograms [15], [16], [20], [25]. Both the G' and G'' elastograms created in this study typically support this theory showing reduced artefacts following MDEV inversion

in comparison to DI. MDEV was not though, able to remove artefacts completely: in instances where the artefact at a single frequency through DI was particularly prominent, such as in the G'' elastograms at 50 Hz (figure 8), this artefact was also present in the MDEV elastogram. It is likely that utilising more frequencies in the MDEV inversion would counter this problem, however, whilst there is no theoretical limit to the number of frequencies used in MDEV, this presents a practical limitation *in vivo* where increasing the number of frequencies increases scan time.

Despite improving image quality the data here suggested that MDEV is unable to improve accuracy in comparison to all three frequencies when analysed independently using DI. Moreover, it was not able to accurately resolve smaller inserts, both in terms of their diameter and radius, better than DI. In these regards it suffers from the same limitations as DI, since it is derived from the same basic assumptions [15]: both DI and MDEV utilise the Laplace operator which functions over a limited voxel range, thereby automatically assuming that local wave propagation is dependent upon the local material properties alone. Comparison of the displacements and corresponding G' elastograms from various length inserts demonstrate that this is not the case (figure 11).

Previous studies have suggested that the compressional wave is likely to have an impact on the accuracy of the inversion [21], [26]. Estimations of the contribution of the compressional wave to the overall displacement demonstrate that contribution of the shear wave was dominant in all simulations. Furthermore, the compressional wave is often discounted from the inversion algorithm because its wavelength is so much greater than that of the shear wave, thus the contribution to the overall displacement term is negligible in comparison. Typically there was little spatial correlation
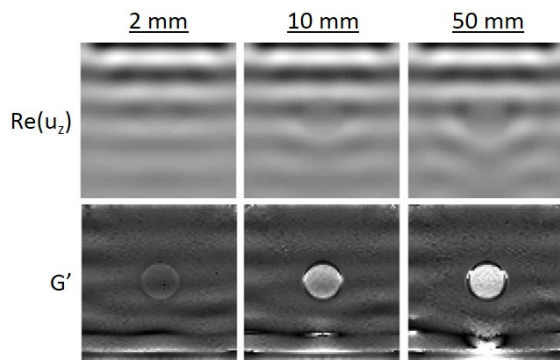
Fig. 11.   Real component of the displacements and corresponding G' elastogram for the 2 mm, 10 mm and 50 mm length inserts of radius 10 mm and prescribed shear modulus 9 kPa for the 100 Hz vibrations. Although in the selected slice through the model the material properties are the same for all three insert lengths, there are clear differences in the displacement maps and corresponding elastograms. This demonstrates breaking of the local homogeneity assumption used in the derivation of the DI algorithm.

between artefacts in the elastogram and high fractional contribution of the compressional wave, with correlations only occuring in a small number of models. In these instances the correlations were towards the lower regions of the model, and outside the regions of interest defined in this study. This suggested that inaccuracies in measurements made by the inversion algorithm were largely down to factors other than the compresssional wave. Whilst the compressional wave may have limited effect on the accuracy of the inversion algorithm *in silico*, it is recognised that there is likely to be greater scattering and mode conversion at interfaces *in vivo* that will increase the influence of the compressional wave.

The simulations used in this study suggest that the minimum length that can accurately be resolved is 20 mm, whilst the minimum radius is 10 mm, though these values are dependent upon the frequency of the induced vibrations and the shear modulus of the insert. It should however be recognised that the sizes at which accurate resolution can be achieved are likely to be greater *in vivo* for several reasons. Firstly, to reduce the impact of discretisation errors from the inversion algorithm [14] a pixel size of 1 mm, lower than can typically be achieved in MRE, was utilised. Additionally, since the aim of the study was to test the inversion algorithms alone, and because synthetic data created with FEA does not suffer from noise, bandpass filters have not been applied to the data. As such, whilst previous research using MDEV has demonstrated excellent detail in the elastograms, measurements from smaller regions should be treated with caution.

The material properties utilised in this study were selected to allow a direct comparison between DI and MDEV. It is however recognised that material properties *in vivo* are likely to correspond to more complex material models [27], which limit the applicability of MRE in the clinic. Whilst MDEV aims to address this issue by reducing these complex models to two frequency independent parameters, further research is warranted to investigate the relationship between these MDEV parameters and the material model.

V. CONCLUSION

MDEV reduces frequency dependent artefacts to produce higher quality elastograms in comparison to DI but is unable

to improve accuracy of the material property measurements.

APPENDIX

The datasets used in this study are publicly available at:

https://github.com/lyamhollis/wave_library

The waves for each simulation are stored in .mat files each containing three 4-D (x,y,z,t) objects: *wx*, *wy* and *wz* corresponding to the displacements in the *x*-, *y*- and *z*-directions respectively.

REFERENCES

[1] R Muthupillai, DJ Lomas, PJ Rossman, JF Greenleaf, A Manduca, and RL Ehman. "Magnetic resonance elastography by direct visualization of propagating acoustic strain waves.". *Science*, vol. 269, no. 5232, pp. 1854-1857, 1995.
[2] R Muthupillai, PJ Rossman, DJ Lomas, JF Greenleaf, SJ Riederer, and RL Ehman. "Magnetic resonance imaging of transverse acoustic strain waves." *Magnet Reson Med*, vol. 36, no.2, pp. 266-274, 1996.
[3] SK Venkatesh, M Yin, and RL Ehman. "Magnetic resonance elastography of liver: technique, analysis, and clinical applications." *J Magn Reson Im*, vol. 37, no. 3, pp. 544–55, 2013.
[4] L Huwart, C Sempoux, E Vicaut, N Salameh, L Annet, E Danse, F Peeters, LC ter Beek, J Rahier, R Sinkus, Y Horsmans, and BE Van Beers. "Magnetic resonance elastography for the noninvasive staging of liver fibrosis." *Gastroenterology*, vol. 135, no. 1, pp. 32-40, 2008.
[5] O Rouvière, R Souchon, G Pagnoux, JM Ménager, and JY Chapelon. "MR Elastography of the kidneys: feasibility and reproducibility in young healthy adults." *J Magn Reson Im*, vol. 34, no. 4, pp. 880-886, 2012.
[6] E Barnhill, P Kennedy, S Hammer, EJR van Beek, C Brown, and NR Roberts. "Statistical mapping of the effect of knee extension on thigh muscle viscoelastic properties using magnetic resonance elastography." *Physiol Meas*, vol. 34, no. 12, pp. 1675-1698, 2013.
[7] A Kolipaka, KP McGee, A Manduca, AJ Romano, KJ Glaser, PA Araoz, and RL Ehman. "Magnetic resonance elastography: Inversions in bounded media." *Magnet Reson Med*, vol. 62, no. 6, pp. 1533-1542, 2009.
[8] A Kolipaka, D Woodrum, PA Araoz, and RL Ehman. "MR elastography of the in vivo abdominal aorta: a feasibility study for comparing aortic stiffness between hypertensives and normotensives." *J Magn Reson Im*, vol. 35, no. 3, pp. 582-586, 2012.
[9] AR Damughatla, B Raterman, T Sharkey-Toppen, N Jin, OP Simonetti, RD White, and A Kolipaka. "Quantification of aortic stiffness using MR elastography and its comparison to MRI-based pulse wave velocity." *J Magn Reson Im*, vol. 41, no. 1, pp. 44-51, 2015.
[10] WE Kenyhercz, B Raterman, VSP Illapani, J Dowell, X Mo, RD White, and A Kolipaka. "Quantification of aortic stiffness using magnetic resonance elastography: Measurement reproducibility, pulse wave velocity comparison, changes over cardiac cycle, and relationship with age." *Magnet Reson Med*, 2015.
[11] A Manduca, TE Oliphant, MA Dresner, JL Mahowald, SA Kruse, E Amromin, JP Felmlee, JF Greenleaf, and RL Ehman. "Magnetic resonance elastography: non-invasive mapping of tissue elasticity." *Med Image Anal*, vol. 5, no. 4, pp. 237-254, 2001.
[12] BN Li, CK Chui, SH Ong, T Numano, T Washio, K Homma, S Chang, S Venkatesh, and E Kobayashi. "Modeling shear modulus distribution in magnetic resonance elastography with piecewise constant level sets." *Magn Reson Imaging*, vol. 30, no. 3, pp. 390-401, 2012.
[13] PR Perriez, FE Kennedy, EEW Van Houten, JB Weaver, and KD Paulsen. "Magnetic Resonance Poroelastography: An Algorithm for Estimating the Mechanical Properties of Fluid-Saturated Soft Tissues." *IEEE Transactions on Medical Imaging*, vol. 29, no. 3, pp. 746-755, 2010.
[14] S Papazoglou, U Hamhaber, J Braun, and I Sack. "Algebraic Helmholtz inversion in planar magnetic resonance elastography." *Phys Med Biol*, vol. 53, no. 12, pp. 3147-3158, 2008.
[15] S Papazoglou, S Hirsch, J Braun, and I Sack. "Multifrequency inversion in magnetic resonance elastography." *Phys Med Biol*, vol. 57, no.8, pp. 2329-2346, 2012.
[16] J Braun, J Guo, R Lützkendorf, J Stadler, S Papazoglou, S Hirsch, I Sack, and J Bernarding. "High-resolution mechanical imaging of the human brain by three-dimensional multifrequency magnetic resonance elastography at 7T." *Neuroimage*, vol. 90, pp. 308-314, 2014.

[17] LEJ Thomas-Seale, D Klatt, P Pankaj, N Roberts, I Sack, and P Hoskins. "A simulation of the magnetic resonance elastography steady state wave response through idealised atherosclerotic plaques." *IAENG International Journal of Computer Science*, vol. 38, no. 4, pp. 394-400, 2011.

[18] TT Dao, P Pouletaut, F Charleux, MHB Tho, and S Bensamoun. "Analysis of shear wave propagation derived from MR elastography in 3D thigh skeletal muscle using subject specific finite element model." In *Conference Proceedings of IEEE Eng Med Biol Soc*, pp. 4026-4029, 2014.

[19] DM McGrath, N Ravikumar, ID Wilkinson, AF Frangi, and ZA Taylor. "Magnetic resonance elastography of the brain: An in silico study to determine the influence of cranial anatomy." *Magn Reson Imaging*, 2015.

[20] S Hirsch, J Guo, R Reiter, S Papazoglou, T Kroencke, J Braun, and I Sack. "MR Elastography of the Liver and the Spleen Using a Piezoelectric Driver, Single-Shot Wave-Field Acquisition, and Multifrequency Dual Parameter Reconstruction." *Magnet Reson Med*, vol. 71, no. 1, pp. 267-277, 2014.

[21] R Sinkus, JL Daire, BE Van Beers, and V Vilgrain. "Elasticity reconstruction: Beyond the assumption of local homogeneity." *Comptes Rendus Mécanique*, vol. 338, no. 7-8, pp. 474-479, 2010.

[22] H Ghasemzadeh and AA Abounouri. "Compressional and shear wave intrinsic attenuation and velocity in partially saturated soils." *Soil Dyn Earthq Eng*, vol. 51, pp. 1-8, 2013.

[23] R Sun, J Chow, and KJ Chen. "Phase correction in separating P- and S-waves in elastic data." *Geophysics*, vol. 66, no. 5, pp. 1515-1518, 2001.

[24] R Sun, GA McMechan, and HH Chuang. "Amplitude balancing in separating P- and S-waves in 2D and 3D elastic seismic data." *Geophysics*, vol. 76, no.3, pp. 103-113, 2011.

[25] J Guo, S Hirsch, A Fehlner, S Papazoglou, M Scheel, J Braun, and I Sack. "Towards an elastographic atlas of brain anatomy." *PloS One*, vol. 8, no. 8, e. 71807, 2013.

[26] R Sinkus, K Siegmann, T Xydeas, M Tanter, C Claussen, and M Fink. "MR elastography of breast lesions: understanding the solid/liquid duality can improve the specificity of contrast-enhanced MR mammography." *Magn Reson Imaging*, vol. 58, no. 6, pp. 1135-1144, 2007.

[27] D Klatt, U Hamhaber, P Asbach, J Braun, and I Sack. "Noninvasive assessment of the rheological behavior of human organs using multifrequency MR elastography: a study of brain and liver viscoelasticity." *Phys Med Biol*, vol. 52, no. 24, pp. 7281-7294, 2007.